J Ther Eng, Vol. 7, Supp 14, pp. 2001–2016, December 2021

Journal of Thermal Engineering
Web page info: https://jten.yildiz.edu.tr
DOI: 10.18186/thermal.1051294

Journal of Thermal Engineering

Research Article

# No formation and its reduction through co-flow methane reburn in a pulverised coal combustion process under various overall equivalence ratio

**Ajay Ku SAHU**[1], **Prakash GHOSE**[1,*]

[1]*School of Mechanical Engineering, KIIT Deemed to be University, Bhubaneswar, India*

## ARTICLE INFO

*Article history*
Received: 31 August 2020
Accepted: 04 November 2020

**Keywords:**
Pulverized Coal; Combustion; Equivalence Ratio; Co-flow Methane; Reburn

## ABSTRACT

Computational simulation has been carried out to investigate the NO formation/depletion in pulverized coal combustion process. Newlands Bituminous coal is injected along with career air through a central hole of an axi-symmetric burner. A certain amount of co-flow methane is injected coaxially as reburn fuel. The effect of overall equivalence ratio on NO formation and NO reburn are mainly focused in this study. Species concentration for various species are also investigated, because both NO formation and depletion are related closely to various species concentration. From the study it is observed that, at overall equivalence ratio φ = 0.8 and 1.0, although the rate of Thermal-NO, Prompt-NO and Fuel-NO formation is high but due to narrow reaction zone and higher air velocity, a weak NO concentration field is observed. On the other hand, a higher NO concentration has been observed with higher equivalence ratio (ratio φ = 3.0, 6.0 and 9.0). It also has been observed, the maximum NO reduction efficiency at φ = 0.8, 1.0 and 3.0 is in between 1% to 7%, whereas for φ = 6.0 and 9.0, the maximum NO reduction efficiency is 27% and 34% respectively. Therefore, co-flow methane injection NO reduction method is more suitable for highly rich mixture conditions. Moreover, the percentage of coal burnout is also relatively higher for higher equivalence ratio condition.

**Cite this article as:** Ajay K S, Prakash G. No formation and its reduction through co-flow methane reburn in a pulverised coal combustion process under various overall equivalence ratio. J Ther Eng 2021;7(Supp 14):2001–2016.

## INTRODUCTION

Coal is the most abundant fuel available on earth. Therefore, it is economical to use in power generation and various metal extraction process. Oxides of nitrogen (NOx), Oxides of sulphur (SOx) and dry and bottom ash are the major pollutants formed during coal combustion. Out of various NOx like NO, $N_2O$ and $NO_2$, NO is the most hazardous and its fraction is higher as compared to other NOx [1]. Presence of nitrogen in coal is a major source of

***Corresponding author.**
*E-mail address: pghosefme@kiit.ac.in, pghoseju@gmail.com

*This paper was recommended for publication in revised form by Regional Editor Chandramohan VP*

NO. It (Fuel-NO) contributes around 50%-60% of total NO [2] for high grade coal. During combustion of high grade coal like bituminous coal, approximately 60% to 70% of inherent nitrogen is converted to NO [3]. Similarly, atmospheric nitrogen causes Thermal-NO formation by reacting with oxygen or hydroxide at a high temperature [4]. Another minor sources of NO are Prompt-NO and $N_2O$ Intermediate NO. It is reported that during bituminous coal combustion up to 30% of total NO may formed due to $N_2O$ intermediate NO [5]. However both Prompt-NO and $N_2O$ intermediate are relatively less important in industrial furnaces due to smaller quantity[6].

Various mechanism are adopted for NO reduction in industrial furnaces such as; Low NOx burner, Over-fire air, NO reburn, Flue gas recirculation, Flame cooling by water or steam injection etc. In low NO burner; the air-fuel mixture is either burnt in fuel-lean condition or fuel rich condition. In fuel-lean condition, excess air and in fuel-rich condition, excess fuel prevents the flame from overheating. As a result the Thermal-NO formation is reduced. On the other hand, with fuel-rich condition, presence of low oxygen minimizes the NO production. Low NOx burner technology is simple and effective and 40%-60% of NO can be reduced by adapting this methodology [7]. Overall equivalence ratio depends on leanness or richness of the mixture. If the mixture is either too lean or too rich, a low temperature flame exists due to the presence of un-burnt reactants. Hence, the Thermal-NO rate decreases. Moreover, rate of reaction for other NO reaction mechanism such as; Prompt-NO and Fuel-NO strongly depends upon temperature also. Therefore, the effect of overall equivalence ratio on NO formation in low NOx burner is an important parameter. Various research works are performed on low NOx burner for coal combustion to investigate the effect of equivalence ratio on NO formation and other combustion characteristics of flame [8, 9]. Hu et al. [10] intensively studied the impact of equivalence ratio on NO formation. They reported that, $NO_x$ emissions increased with increase in equivalence ratio under fuel-lean conditions, then declined dramatically after when equivalence ratio become 0.8.

Fuel biasing is another simple method used to reduce NO. In this method either low nitrogen content fuel or nitrogen free fuel is used as secondary fuel. So that the Fuel-NO can be reduced up to a great extent. Biomass co-firing along with coal is used as a fuel biasing method to minimize NOx [11–13]. The nitrogen free gaseous fuel like methane or natural gas can be a good option of biasing fuel. It has many advantages, viz; (1) Methane is a nitrogen free fuel, so Fuel-NO will be reduced by adding this with coal. (2) Total ash will be reduced with the addition of methane. (3) It can be used as re-burn fuel (re-burn fuel should be highly volatile and reactive). NO re-burn is a methodology where generally either hydrocarbon fuel or ammonia are injected at downstream of the flame. Ammonia injection technology called selective catalytic reactor (SCR) is expensive and required additional fittings. In addition to that ammonia in gaseous form is harmful. Su et al. [14] investigated the NOx destruction through numerical simulation by using pure methane as reburn fuel at downstream. Han et al. [15] used a premixed methane-ammonia blend as reburn fuel for NO reduction, whereas Zarnitz et al. [16] used coal volatile as reburn fuel at downstream of coal burner. Wu et al. [17] investigated the effect of syngas as reburn fuel on NO reduction using both co-flow injection and downstream injection methods. From the investigation it is observed that, 46% NO reduction has been obtained with co-flow reburn fuel injection, whereas by using conventional downstream injection method, only 23% NO reduction has been obtained. From the literature it has been observed that around 30%-40% of NO can be reduced by using reburn fuel at flame downstream. Some of the authors worked on co-flow methane injection in pulverized coal combustion systems experimentally [18] and computationally [19, 20]. But no one investigated the effect of methane on NO reduction rather they used methane as a secondary fuel only.

Therefore in this work, a computational simulation is performed to investigate the effect of overall equivalence ratio on total NO formation and reduction. Thermal-NO, Prompt-NO and Fuel-NO mechanism are incorporated for NO formation calculation. For NO reduction, NO-reburn reaction mechanism is used, where co-flow methane is used as reburn fuel. Both Newlands bituminous coal-air and co-flow methane are injected from the same plane. The mass flow rate of coal and methane are calculated in such a way that, 50% of the total heat is contributed by coal and remaining 50% heat is contributed by methane reaction.

## COMPUTATIONAL MODELLING

### Coal Properties

Newlands bituminous coal is used as base fuel. Various substance obtained from Proximate and Ultimate analysis along with the coal particle size are given in Table 1 [21].

**Table 1.** Proximate and Ultimate analysis data for Newlands Bituminous coal

| Proximate analysis [wt%] | | Ultimate analysis [wt%] | |
|---|---|---|---|
| Volatile matter[b] | 26.90 | Carbon[b] | 71.90 |
| Fixed carbon[b] | 57.90 | Hydrogen[b] | 4.40 |
| Ash[b] | 15.20 | Oxygen[b] | 6.53 |
| Moisture[a] | 2.60 | Nitrogen[b] | 1.50 |
| | | Sulphur[b] | 0.44 |

Higher calorific value 29.1 MJ/kg
Lower calorific value 28.1 MJ/kg
Particle maximum diameter 60 μm
Particle minimum diameter 5 μm
Particle mean diameter 33 μm

The chemical formula for volatile is obtained from Proximate and Ultimate analysis as $C_{4.61}$ $H_{4.94}$ $O_{0.46}$ $N_{0.1219}$ $S_{0.0155}$ [22]. Molecular weight of the volatile and high temperature volatile yielding factor is taken as 70 and 2.3 respectively [23].

**Physical Model and Governing Equations**

A two dimensional geometry is prepared to simulate the combustion process through axi-symmetric burner as shown in Figure. 1 Through the central hole, coal is injected along with primary air. An annular hole is provided for co-flow methane feeding in to the burner. A wide passage is given beyond the methane inlet for free flow of atmospheric air. Since in this work, solid coal particles are injected into the gas phase domain, the problem is solved under the Eulerian-Lgrangian frame of reference. Favre averaged [24] gas phase governing equations for conservation of mass, momentum and general scalar variable are given in Equation (1), (2) and (3) respectively.

**Conservation of mass**

$$\frac{\partial}{\partial x_i}\left(\bar{\rho}\tilde{u}_i\right) = S_m \tag{1}$$

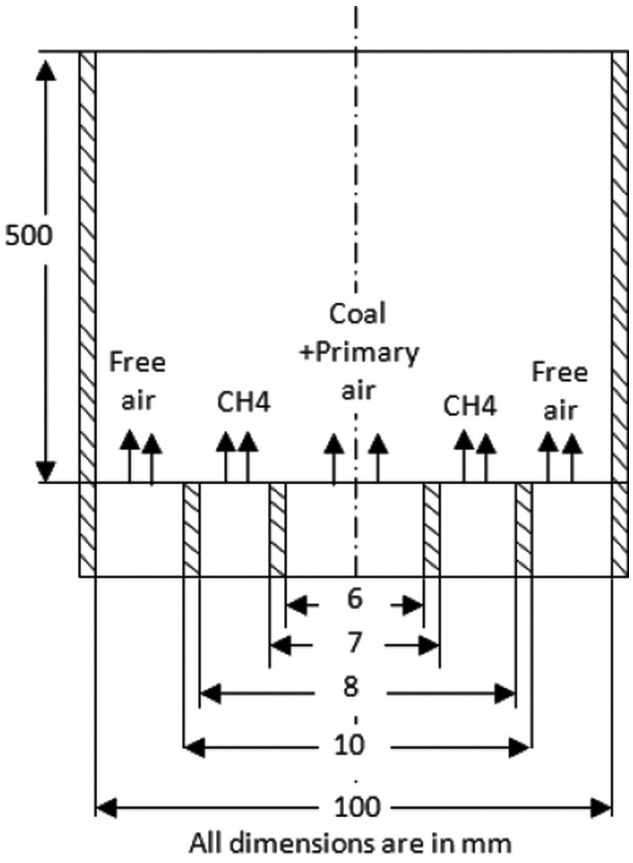


**Figure 1.** Physical geometry.

**Conservation of momentum**

$$\frac{\partial}{\partial x_i}\left(\bar{\rho}\tilde{u}_i\tilde{u}_j\right) = -\frac{\partial \bar{p}}{\partial x_i} + \frac{\partial}{\partial x_i}\left(\bar{\tau}_{ij} - \bar{\rho}\widetilde{u_i'' u_j''}\right) + S_s \tag{2}$$

**Conservation of general scalar variable**

$$\frac{\partial}{\partial x_i}\left(\bar{\rho}\tilde{u}_j\tilde{\varphi}\right) = \frac{\partial}{\partial x_i}\left(\Gamma_{\phi,eff}\frac{\partial \tilde{\varphi}}{\partial x_i}\right) + S_{\varphi,s} \tag{3}$$

Phi ($\varphi$) represents enthalpy in energy equation and species mass fraction for various chemical species in species transport equations. In energy conservation equation, $\Gamma_{\phi,eff} = \left(\Gamma_{\phi,lam} + \Gamma_{\phi,tur}\right) = \left(\frac{\mu}{\sigma} + \frac{\mu_t}{\sigma_t}\right)$ whereas in species conservation equation; $\Gamma_{\phi,eff} = \left(\Gamma_{\phi,lam} + \Gamma_{\phi,tur}\right) = \left(\frac{\mu}{Sc} + \frac{\mu_t}{Sc_t}\right)$..

To evaluate Reynolds stresses present in momentum equations, Boussinesq hypothesis is used as;

$$-\bar{\rho}\widetilde{u_i'' u_j''} = \mu_t\left(\frac{\partial \tilde{u}_i}{\partial x_j} + \frac{\partial \tilde{u}_j}{\partial x_i}\right) - \frac{2}{3}\bar{\rho}\tilde{k}\delta_{ij} \tag{4}$$

Where, $\mu_t = \rho C_\mu \frac{k^2}{\varepsilon}$. In order to calculate eddy viscosity and Reynold stresses, transport equation for $k$, $\varepsilon$ are solved by using Standard $k$-$\varepsilon$ model [25]. Required boundary conditions are given at different boundaries for initializations of $k$ and $\varepsilon$. The inter-phase source terms for different governing equations are discussed in following sections.

**Discrete Phase Model**

A finite number of coal particles having diameter range given in Table 1. are injected through primary air hole. The spread parameter of 4.02 is used to calculate particle diameter distribution by following Rosin-Rammler distribution scheme [26]. The turbulent interaction in between gas and particle phase are simulated by employing Discrete random walk model [27]. A force balance equation is solved to evaluate the drag force exerted on droplet by gas phase and vice versa is expressed as;

$$m_p(j)\frac{du_{p_i}}{dt} = \frac{\pi}{8}\rho_p\left[d(j)\right]^2 \left|u_i - u_{p_i}(j)\right|\left[u_i - u_{p_i}(j)\right]C_{drag} \tag{5}$$

In equation (5) the drag coefficient is calculated by following the spherical drag law [28], expressed as; $C_{drag} = a_1 + \frac{a_2}{Re} + \frac{a_3}{Re^2}$, where $a_1$, $a_2$, $a_3$ are model constants

and $Re\left(=\frac{\rho\left|u_i-u_{p_i}(j)\right|d_j}{\mu}\right)$ is the Reynolds number considering the flow over spherical particles.

A mass balance equation is solved to incorporate the exchange of mass in between two phases because of volatile evolution and char combustion is expressed as;

$$\frac{\mathrm{dm_p(j)}}{\mathrm{dt}}=\frac{\mathrm{dm_{vol}(j)}}{\mathrm{dt}}+\frac{\mathrm{dm_{char}(j)}}{\mathrm{dt}} \tag{6}$$

where $\frac{\mathrm{dm_{vol}(j)}}{\mathrm{dt}}$ and $\frac{\mathrm{dm_{char}(j)}}{\mathrm{dt}}$ are volatile evolution rate and char combustion rate respectively are expressed mathematically in the following sections.

An energy balance equation is solved to include the heat energy exchanges in between gas and particle phases because of convection, radiation and coal burnout. The energy balance equation is expressed as;

$$m_p(j)c_{p_g}\frac{dT_p}{dt}=h_cA_p\left(T-T_p\right)+\varepsilon_pA_p\sigma\left(\theta_R^4-T_p^4\right)-f_h\left(\frac{dm_{vol}(j)}{dt}\Delta H_v+\frac{dm_{char}(j)}{dt}\Delta H_c\right) \tag{7}$$

In the convective part of equation (7), the heat transfer coefficient is evaluated by using Nusselt number correlation suggested by Ranz and Marshal [29]. A large amount of heat is radiated from the flame due to high flame temperature. In addition to that, presence of soot in flame radiated significantly larger amount of heat from the flame. Considering bulk gas as participating media, Discrete Ordinate (DO) [30] radiation modelling method is employed to solve the radiative transport equation. From the solution, the radiative temperature $\theta_R$ is calculated as; $\theta_R=\left(\frac{\int_{\Omega=4\pi}\mathrm{Id}\Omega}{4\sigma}\right)^{1/4}$.

A RTE (Radiative Transport Equation) is solved to evaluate radiation intensity. Weighted sum gray gas model (WSGGM) [31] is used to determine the bulk gas absorption coefficient. The absorption coefficient in gas phase includes the effect of absorptivity of soot as well. Scattering and radiative transmission is neglected in gas phase, whereas absorption and scattering both are considered for particle phase. The last term in the equation (7) is the heat transfer from particle surface due to volatile and char combustion. Khan and Greeves soot model [32] is used to include the effect of soot on field temperature.

**Reaction Modelling**

The rate of evolution of volatile matter is calculated with the help of single rate kinetic model [33] expressed as;

$$\frac{\mathrm{dm_{vol}(j)}}{\mathrm{dt}}=k\left[m_p-\left(1-\mathrm{P_{vol_0}}\right)m_{p0}\right] \tag{8}$$

In equation (8), the kinetic rate coefficient is evaluated as; $k=Ae^{-(E/RT)}$, where pre exponential factor $A=4.747\times10^5$ and activation energy $E=7.4\times10^6$. Intrinsic char reaction model [34] is used to predict the char combustion rate. The rate of depletion of char particle mass is expressed as;

$$\frac{\mathrm{dm_{char}(j)}}{\mathrm{dt}}=-\mathrm{A_p}\frac{\rho\mathrm{RTY_{ox}}}{\mathrm{MW_{O_2}}}\frac{\mathrm{D_0}\Re}{\mathrm{D_0}+\Re} \tag{9}$$

In this model the reaction rate depends on both oxygen diffusion rate towards the core and finite rate of reaction between carbon and oxidant including the effect of coal porosity and porous hole twist as well. In equation (9), $D_0$ and $\Re$ denoted the oxidant diffusion rate coefficient and chemical reaction rate considering physical nature of the coal respectively and $A_p$ is the particle surface area.

Reaction mechanisms with four reactions are considered for either gas phase reaction or particle phase reaction given as following;

$$\mathrm{C_{4.61}H_{4.94}O_{0.46}N_{0.1219}S_{0.0155}+3.32O_2\rightarrow4.61CO+2.47H_2O+0.0609N_2+0.0155SO_2} \tag{R-1}$$

$$\mathrm{CH_4+1.5O_2\rightarrow2H_2O+CO} \tag{R-2}$$

$$\mathrm{C(char)+0.5O_2\rightarrow CO} \tag{R-3}$$

$$\mathrm{CO+1/2O_2\rightarrow CO_2} \tag{R-4}$$

For gas phase combustion, Eddy dissipation model proposed by Magnussen and Hjertager [35] is used. The reaction rate in gas phase combustion is evaluated by considering the smallest rate of reaction out of three as;

$$\tilde{\omega}_{EDM}=B\bar{\rho}\frac{\varepsilon}{k}min\left\{\tilde{Y}_f,\frac{\tilde{Y}_{O_2}}{\gamma},\frac{B_1\sum\tilde{Y}_p}{1+\gamma}\right\} \tag{10}$$

In this model $B$ and $B_1$ are the model constants and their value are taken as 4 and 0.5 respectively. $\tilde{Y}_f$, $\tilde{Y}_{o_2}$, $\tilde{Y}_p$ and $\gamma$ are mass fraction of fuel, oxygen, products and local equivalence ratio.

**NOx Modelling**

During combustion of hydrocarbon fuel, a big amount of pollutant NO formation occurs as compared to other NOx such as; $N_2O$ and $NO_2$ [1]. Therefore only NO formation has been considered in this work. Moreover the effect of reburn on net NO is also considered by using co-flow methane as reburn fuel.

Thermal-NO, Prompt-NO (originates from atmospheric nitrogen) and Fuel-NO (originated from inherent nitrogen stored in fuel) are considered as the source of NO. Thermal-NO formation is evaluated by following the well known Zeldovich mechanism [36]. By considering the Quasi-steady assumption of nitrogen atom formation, the rate of Thermal-NO is expressed as;

$$\frac{d[NO]}{dt} = 2k_{f,1}\left[X_O\right]\left[X_{N_2}\right] \frac{\left(1-\frac{k_{r,1}k_{r,2}\left[X_{NO}\right]^2}{k_{f,1}\left[X_{N_2}\right]k_{f,2}\left[X_{O_2}\right]}\right)}{\left(1+\frac{k_{r,1}\left[X_{NO}\right]}{k_{f,2}\left[X_{O_2}\right]+k_{f,3}\left[X_{OH}\right]}\right)} \text{mol/m}^3-\text{s} \quad (11)$$

where molar concentration of $O$ and $OH$ are evaluated as; $\left[X_O\right]=3.97\times10^5 T^{-1/2} exp^{-31090/T}\left[X_{O_2}\right]^{1/2}$ and $\left[X_{OH}\right]=2.129\times10^2 T^{-0.57} exp^{-4595/T}\left[X_O\right]^{1/2}\left[X_{H_2O}\right]^{1/2}$ respectively [37].

The reaction in between hydrocarbon radicals and atmospheric nitrogen within the fuel rich zone under moderate temperature forms Prompt-NO. The rate of Prompt-NO proposed by De Soete [38] is expressed as;

$$\frac{d[NO]}{dt} = fk_{pr}[X_{O_2}]^a[X_{N_2}][X_{fuel}]\,exp^{-E_a/RT} \quad (12)$$

In equation (12), $f$ is a correction factor that depends on carbon atom number of fuel and the equivalence ratio within the reaction zone. $k_{pr}$ is the NO production rate coefficient. $a$ is reaction order for oxygen depends up on the oxygen molar fraction within the reaction zone.

During the reaction, fuel nitrogen converted into intermediate species like HCN and $NH_3$. The consequent reaction forms NO by reacting with $O_2$. Also a part of NO reacted with HCN/$NH_3$ again converted to $N_2$. However a significant amount of fuel N also directly converts to NO. The source term for HCN, $NH_3$ and NO (formation of HCN,$NH_3$ and NO from fuel nitrogen conversion) in their corresponding species transport equations are expressed in ref. [36]. The HCN and $NH_3$ depletion rate by reacting with $O_2$ and $N_2$ or formation of NO are expressed as;

$$\frac{d[HCN]}{dt}\Big|_{O_2\to NO} = k_1\left[X_{HCN}\right]\left[X_{O_2}\right]^a e^{-E_1/RT}\frac{MW_{NO}p}{R\bar{T}} \quad (13a)$$

$$\frac{d[HCN]}{dt}\Big|_{NO\to N_2} = -k_2\left[X_{HCN}\right]\left[X_{NO}\right]e^{-E_2/RT}\frac{MW_{NO}p}{R\bar{T}} \quad (13b)$$

$$\frac{d[NH_3]}{dt}\Big|_{O_2\to NO} = k_3\left[X_{NH_3}\right]\left[X_{O_2}\right]^a e^{-E_3/RT}\frac{MW_{NO}p}{R\bar{T}} \quad (13c)$$

$$\frac{d[NH_3]}{dt}\Big|_{NO\to N_2} = -k_4\left[X_{NH_3}\right]\left[X_{NO}\right]e^{-E_4/RT}\frac{MW_{NO}p}{R\bar{T}} \quad (13d)$$

In this work, the nitrogen contained by volatile and char are taken as 30% and 70% respectively. It is considered that 90% nitrogen convertible to form NO. 80% and 20% of volatile N is allowed to convert HCN and $NH_3$ respectively, whereas direct conversion of volatile N to NO is not considered. 100% of char is converted to direct NO.

However NO concentration also decreases due to the reaction of NO with CH radicals within the fuel rich zone. The reaction mechanism of NO with CH radicals is globally expressed as;

$$CH_i + NO \to HCN + products(H2O, OH, O\ldots etc.) \quad (14)$$

In order to evaluate the NO depletion rate, partial equilibrium approach is used [39], where NO depletion rate and HCN formation rates considering $CH_4$ is reburn fuel are expressed as;

$$\frac{d[HCN]}{dt} = 4\times10^{-4}\left\{\left(k_a\chi_1 + k_b\chi_1^2\right)\left[X_{CH_4}\right]\left[X_{NO}\right]\right\} \quad (15)$$

$$\frac{d[NO]}{dt} = -4\times10^{-4}\left\{\left(k_a\chi_1 + k_b\chi_1^2\right)\left[X_{CH_4}\right]\left[X_{NO}\right] + \left(k_c\chi_1^3\chi_2\right)\left[X_{CH_4}\right]\left[X_{NO}\right]\right\} \quad (16)$$

where $\chi_1 = \frac{X_H}{X_{H_2}}$; Its value is taken as one by assuming that hydrogen radical H is observed as same order with $H_2$ near post flame region in non premixed flame. $\chi_2 = \frac{X_{OH}}{X_{H_2O}}$, where mole fraction of OH radical is obtained from the reaction;

$$OH + H_2 \overset{k_{f1},\ k_{r1}}{\leftrightarrow} H_2O + H \quad (17)$$

The rate constants $k_a$, $k_b$, $k_c$, $k_{f1}$, $k_{r1}$ in equation (15) and (16) for different re-burn fuel are used from the work Leung et al. [40].

## OPERATING CONDITIONS

Five different overall equivalence ratio conditions have been used in this study as mentioned in Table 2. In all the cases, mass flow rate of coal and methane are kept constant.

By changing the primary air mass flow rate the desired overall equivalence ratio is maintained. However, the coal mass flow and methane mass flow rate are taken in such a way that the heat input by both the fuel are in 50:50 ratio. For the calculations, higher calorific values of coal and methane are used. The higher calorific values of coal and methane are taken as 29MJ/kg and 50MJ/kg respectively. The mass of fuel supplied are calculated as;

$$m_{coal} = \frac{Total\,heating\,value(5kW) \times heat\,input\,percentage\,from\,coal}{Calorific\,value\,of\,coal} \quad (17)$$

$$m_{methane} = \frac{Total\,heating\,value(5kW) \times heat\,input\,percentage\,from\,methane}{Calorific\,value\,of\,methane} \quad (18)$$

The mass of air supplied is calculated as;

$$Equivaleance\,ratio = \frac{\left(\frac{m_f}{m_a}\right)_{actual}}{\left(\frac{m_f}{m_a}\right)_{stoich}} \quad (19)$$

where mass flow rate of fuel $m_f = m_{coal} + m_{methane}$ and stoichiometric fuel-air ratio is calculated as;

$$\left(\frac{m_f}{m_a}\right)_{stoich} = \frac{m_{CH_4} + m_C + m_{vol}}{m_{a\to CH_4} + m_{a\to C} + m_{a\to vol}} \quad (20)$$

In equation (20), $m_{a\to CH_4}$, $m_{a\to C}$ and $m_{a\to vol}$ are the mass of air required to completely burn a mass of fuel $m_{CH_4}$, $m_C$ and $m_{vol}$ respectively, which are calculated by using the molar coefficient and molecular weight of the fuel and oxidant.

## RESULTS AND DISCUSSION

### Model Validation

In order to establish the acceptability of current computational model, few results are compared with an experimental work performed in Japanese Central Research Institute of Electric Power Industry (CRIEPI) [21]. An axisymmetric model is prepared with same dimension as mentioned in the experimental set up. Same inlet conditions are used as mentioned. A parabolic velocity profile for main air is used by keeping given mass flow rate unchanged. Newlands Bituminous coal is used as fuel along with coflow methane pilot fuel. The various computational models has been used in this work are discussed in computational modelling section. The experimental conditions are given in Table 3.

## GRID INDEPENDENT TEST

Grid independent test has been carried out using three different mesh configuration such as; 60000, 40000 and 30000 mesh. Quadrilateral structured elements are used throughout the computational domain. Nitrogen and volatile matter concentration along the axis with different mesh configuration at overall equivalence ration φ = 9.0 are compared as shown in Figure 3. Both $N_2$ and volatile concentration deviates significantly throughout the length with 30000 meshes as compared to 40000 and 60000 meshes. On the other hand, minor deviation in both $N_2$ and volatile concentration has been observed between 40000 and 60000 mesh configured computational domain. However, for the entire simulation 60000 mesh size computational domain is used for simulation.

**Table 3.** Experimental conditions [21]

| **Bulk equivalence ratio** | **6.09** |
|---|---|
| Pulverised-coal feed rate | $1.49 \times 10^{-4}$ kg/s |
| Air flow rate | $1.80 \times 10^{-4}$ m$^3$/s |
| Methane flow rate | $2.33 \times 10^{-5}$ m$^3$/s |
| Reynolds number | 2544 |

**Table 2.** Operating conditions

| **Case** | **Heat percentage ratio (Total heat 5 kW) Coal: Methane** | **Equivalence ratio** | **Coal mass flow rate (kg/s)** | **Methane mass flow rate (kg/s)** | **Primary air mass flow rate (kg/s)** |
|---|---|---|---|---|---|
| Case A | 50:50 | 0.8 | $8.896 \times 10^{-05}$ | $5 \times 10^{-05}$ | $2.105 \times 10^{-03}$ |
| Case B | | 1 | $8.896 \times 10^{-05}$ | $5 \times 10^{-05}$ | $1.684 \times 10^{-03}$ |
| Case C | | 3 | $8.896 \times 10^{-05}$ | $5 \times 10^{-05}$ | $5.614 \times 10^{-04}$ |
| Case D | | 6 | $8.896 \times 10^{-05}$ | $5 \times 10^{-05}$ | $2.807 \times 10^{-04}$ |
| Case E | | 9 | $8.896 \times 10^{-05}$ | $5 \times 10^{-05}$ | $1.871 \times 10^{-04}$ |

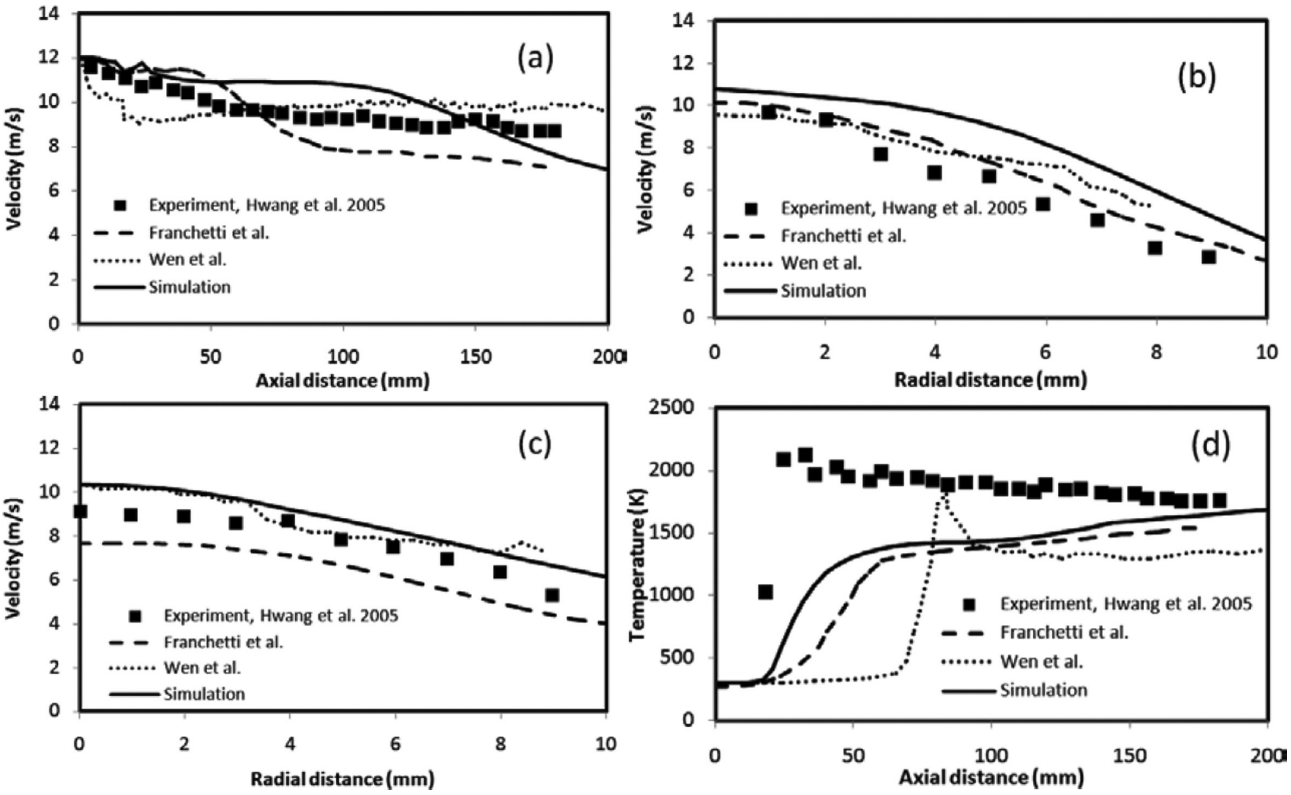


**Figure 2.** Axial velocity distribution, a) along the combustor axis, b) along radial direction at axial position 60 mm from inlet, c) along radial direction at axial distance 120 mm from inlet, d) Temperature comparison along the axis.

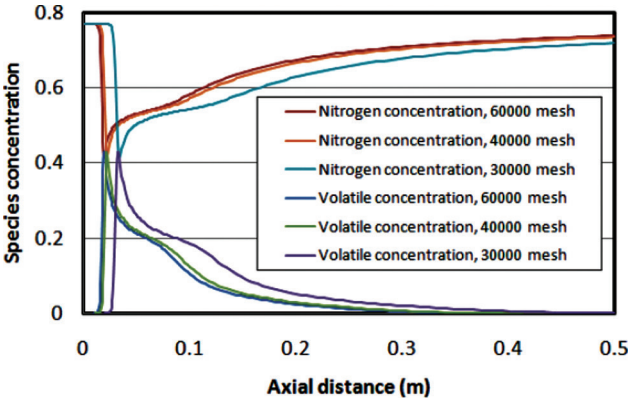


**Figure 3.** Nitrogen and volatile matter concentration along the axis with different mesh configuration at φ = 9.0.

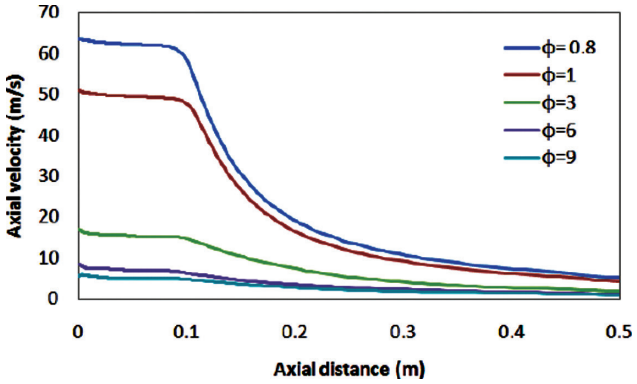


**Figure 4.** Axial velocity at various overall equivalence ratio conditions.

**Species and Temperature Distribution Field**

To increase the overall equivalence ratio, reduced primary air supply is required as given in Table 2. Therefore the primary air velocity is very high at inlet for very low equivalence ratio (0.8 and 1.0). The primary air velocity along the axial line at different overall equivalence ratio is shown in Figure 4.

Figure 5. shows different major species variation along axial direction for various overall equivalence ratio. In all the cases, either a sudden drop or rise of species has been observed near inlet region. The sudden rise of volatile mass little away from inlet indicates the position and intensity of volatile formation rate along the axis. The drooping characteristic of volatile mass fraction line depicts the

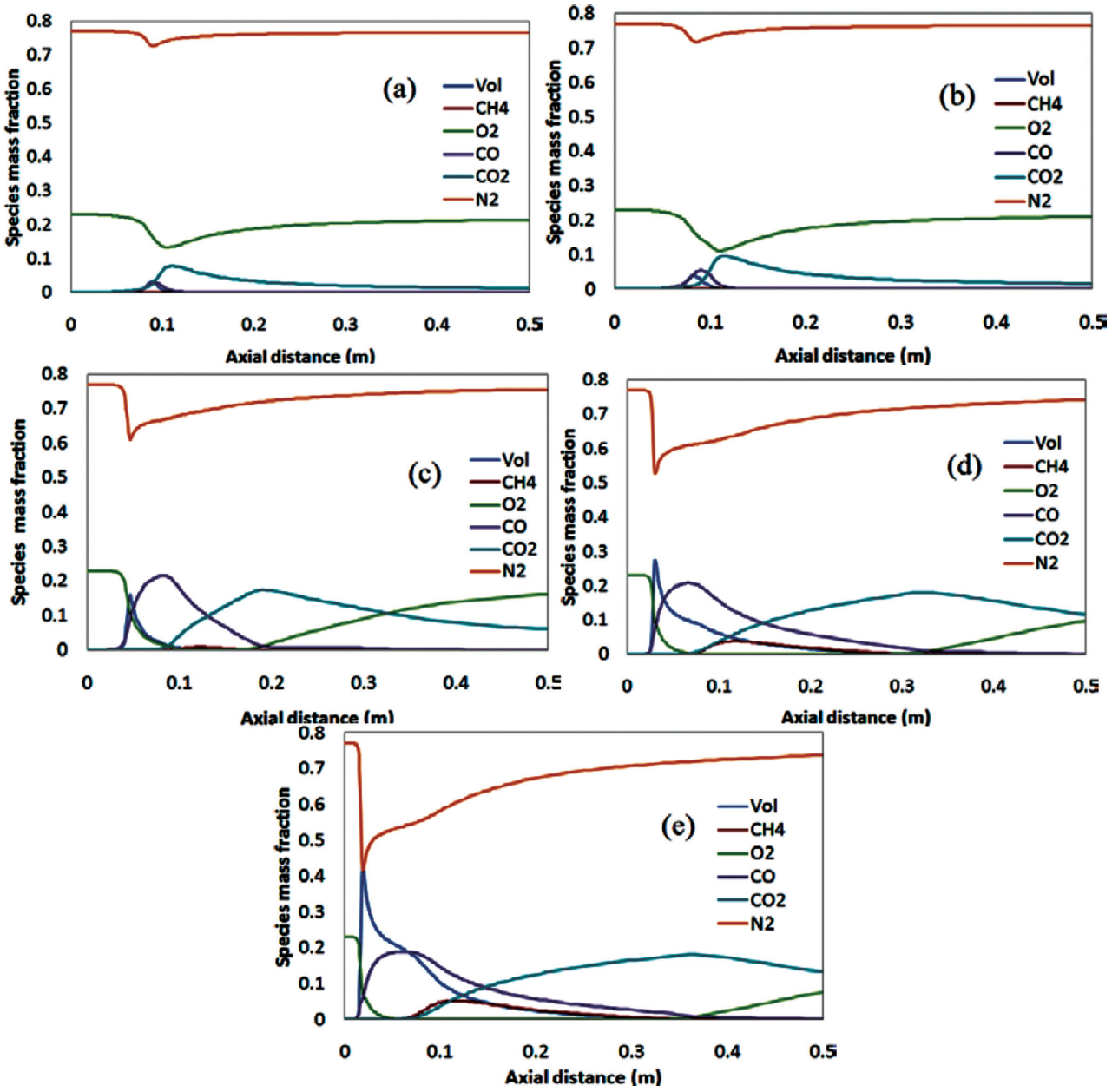


**Figure 5.** Major species concentration along the axial line for a) φ = 0.8, b) φ = 1.0, c) φ = 3.0, d) φ = 6.0, e) φ = 9.0.

diffusion and consumption of this fuel during combustion. Moreover the sudden fall of oxygen at this position confirms the oxidation of volatile. Oxygen consumption and CO evolution (primary reaction) start at this position by following the reaction R-1 and R-2. In secondary reaction, $CO_2$ evolution commences by consuming CO and $O_2$ little away from the primary reaction. However, this necking region becomes closer to inlet with increase in overall equivalence ratio. It is because the low air velocity for higher equivalence ratio could not flow the coal particle quickly out. Therefore the higher residence time of the coal particles within hot region makes a higher evolution of volatile and much closer to inlet region. From Figure 6, where gaseous fuel (volatile and $CH_4$) concentration is illustrated, one can visualise the concentration of volatile with respect to overall equivalence ratio. Relatively a higher concentration $O_2$ has been observed at downstream for lower overall equivalence ratio conditions. Because, in these cases, the excess air that does not participates in reaction, presents at downstream. Moreover, evolution of CO and $CO_2$ from CO starts from the same position for the case of lower equivalence ratio.

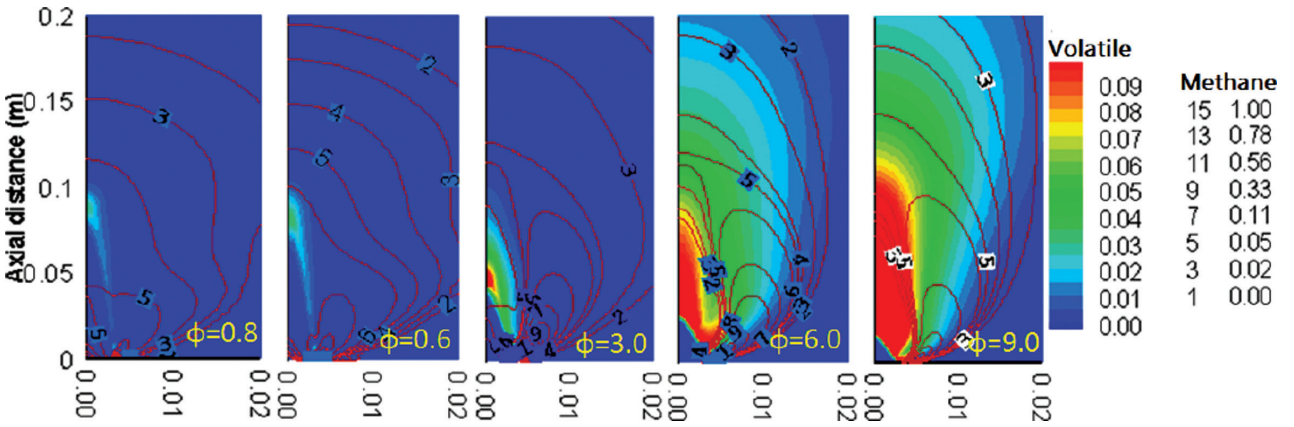


**Figure 6.** Enlarged view of mass fraction contour of volatile and methane for various equivalence ratio condition cases.

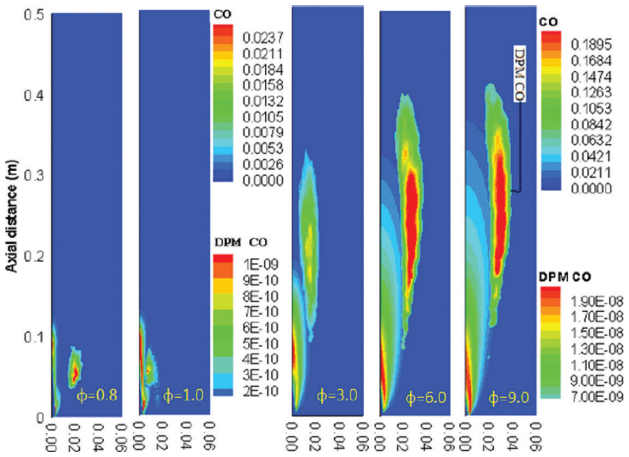


**Figure 7.** Mass fraction of CO for various equivalence ratio condition cases.

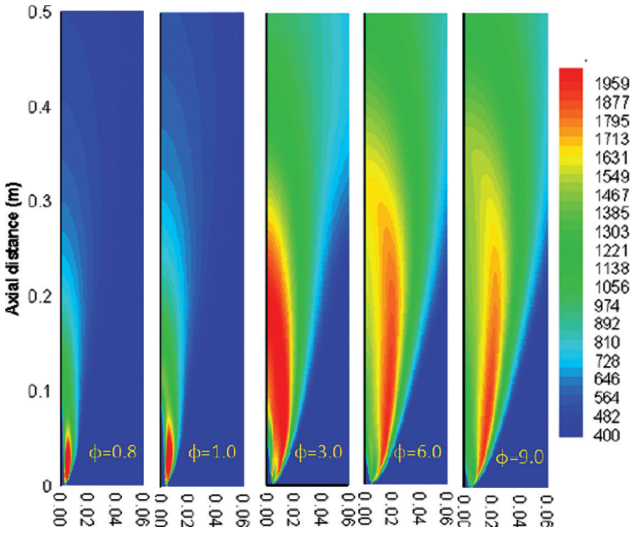


**Figure 8.** Temperature field in degree Kelvin for various equivalence ratio condition cases.

Figure 7, illustrates the CO concentration obtained from primary reaction of gaseous fuel (volatile + $CH_4$) and char as well. The CO concentration for any equivalence ratio obtained from primary reaction of gaseous fuel is visualized closest to the axial line and inlet region. On the other hand CO concentration obtained from primary reaction of char with $O_2$ is shown as DPM CO in this Figure, which concentrates away from axial line and inlet region. It is because, the char reaction occurs after the volatile removal from the coal particles. However CO concentration obtained through gaseous fuel combustion is much higher as compared to CO concentration through char reaction, due to much slower rate of reaction in between char and $O_2$. It is obvious that, rich mixture forms more CO due to the presence of insufficient $O_2$ during reaction. Therefore, with increase in overall equivalence ratio, the CO concentration increases.

Temperature field at different equivalence ratio is shown in Figure 8. Here the total flame temperature is the combine effect of the heat generated from the reactions Equation (1), (2) and (4). With φ=1.0, even though the temperature field is smaller as compared to higher equivalence ratio case, but the peak temperature is the highest ( 2204K). The peak flame temperatures for different cases are given in Table 4. The reason of smaller temperature field at very less equivalence ratio is due to smaller volatile evolution and poor char burnout in these cases because of higher air velocity. At the same time, better air fuel ratio within a limited region gives very high flame temperature. For the case φ = 3.0, higher $O_2$ availability as compared to φ=6.0 and 9.0 and better particle residence time as compared to φ = 0.8 and 1.0, a wide temperature field is observed with maximum temperature of 2091K. Similarly for very high equivalence ratio cases, as equivalence ratio increases, peak flame temperature decreases due to deficit of $O_2$ and the temperature field become spread due to poor transport rate causes by smaller velocity.

## NO FORMATION AND DESTRUCTION

The total NO concentration is the sum of Thermal-NO, Prompt-NO and Fuel-NO concentration. Figure 9, illustrates the total NO concentration field.

Thermal-NO depends upon flame temperature, availability of atmospheric $O_2$ and $N_2$. From Figures 4a-e, it is also observed that, for lower equivalence ratio cases, plenty of atmospheric nitrogen is available in reaction zone. Therefore, due to very high flame temperature and better availability of $O_2$ and $N_2$, a smaller but intense reaction rate for Thermal-NO has been observed at φ=0.8 and 1.0 as shown in Figure 10.

As overall equivalence ratio increases, due to $O_2$ and $N_2$ deficit and decreased flame temperature, the intensity of Thermal-NO formation rate decreases. However for higher equivalence ratio, a wide reaction zone for Thermal-NO has been observed due to a wider higher temperature region in these cases.

Prompt-NO reaction rate is also related to atmospheric $N_2$, where $N_2$ reacts with hydrocarbon radicals to form intermediate species. The consequent reactions of intermediate species with $O_2$ and oxygen radicals form Prompt-NO. Therefore Prompt-NO formation rate become high within the fuel rich zone at moderate temperature. But

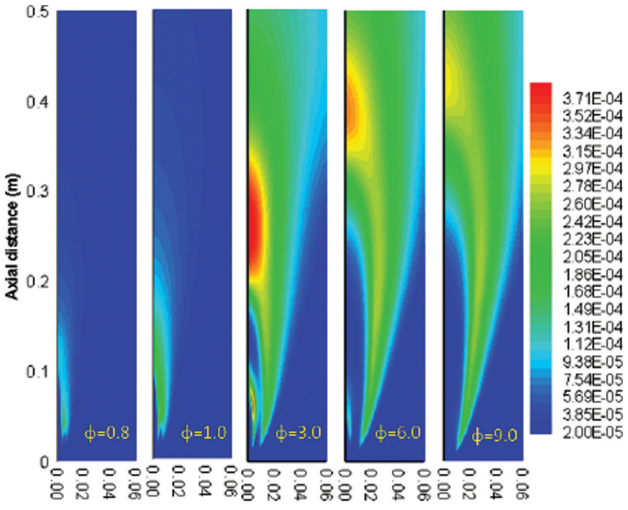


**Figure 9.** Total NO mass concentration for various equivalence ratio condition cases.

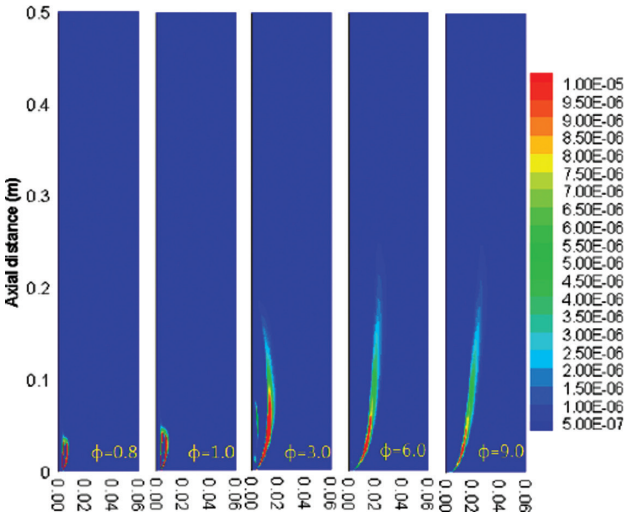


**Figure 11.** Rate of Prompt-NO (kmol/m3-s) contour for various equivalence ratio condition cases.

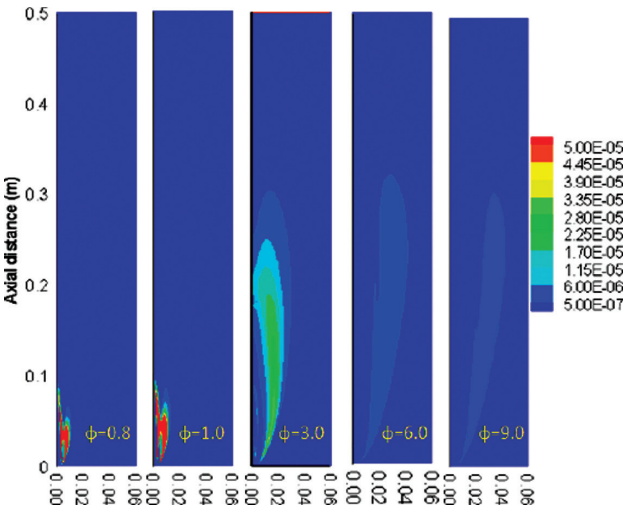


**Figure 10.** Rate of Thermal-NO (kmol/m3-s) contour for various equivalence ratio condition cases.

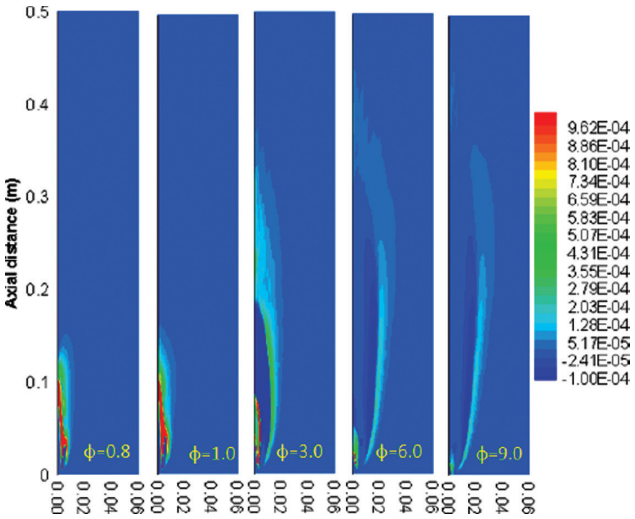


**Figure 12.** Rate of Fuel-NO (kmol/m3-s) contour for various equivalence ratio condition cases.

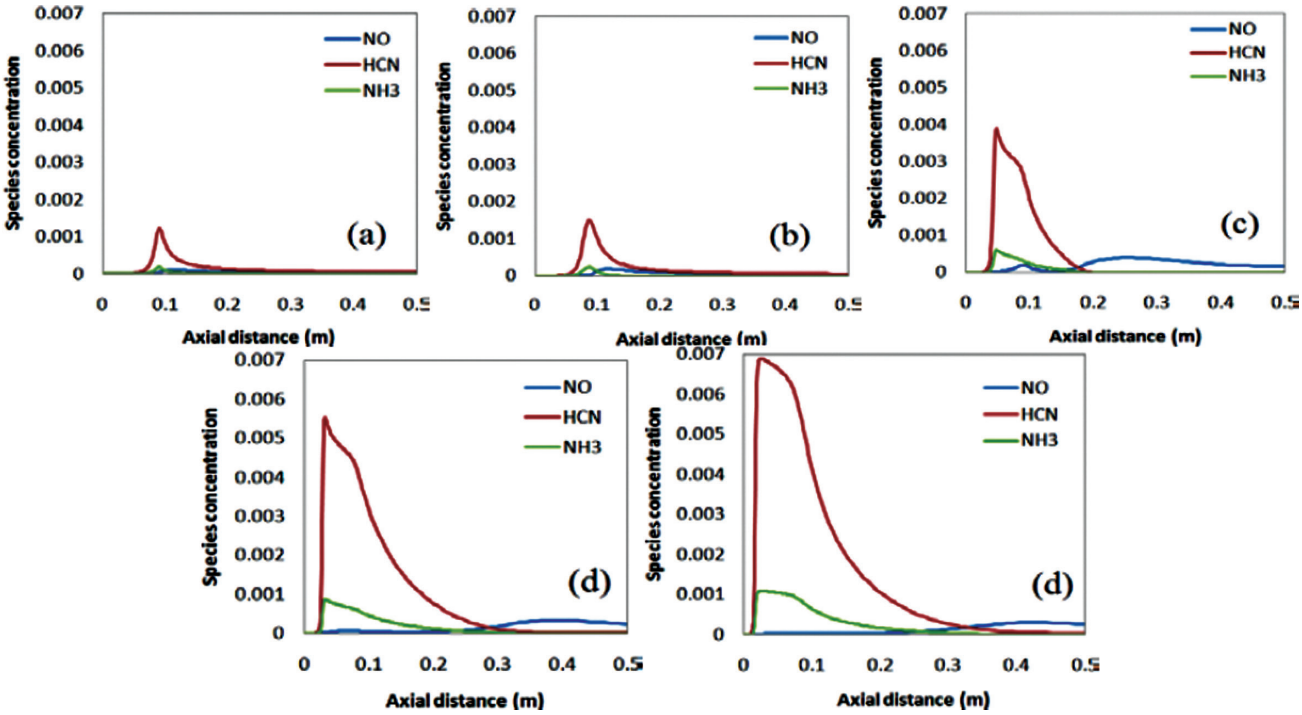


**Figure 13.** a) HCN, NH3 and NO concentration along the axis for a) φ = 0.8 b) φ=1.0 c) φ = 3.0 d) φ = 6.0 e) φ = 9.0.

if local equivalence ratio becomes too high, Prompt-NO decreases due to deficit in $O_2$. Figure 11 illustrates the rate of formation of Prompt-NO at various overall equivalence ratio conditions.

For the cases of low equivalence ratio (φ=0.8 and 1.0), despite of lack of rich local equivalence ratio, sufficient $O_2$ and $N_2$ increases the Prompt-NO formation rate in these cases. On the other hand, as the overall equivalence rate increases, despite of availability of richer equivalence ratio, insufficient $O_2$ and oxygen radicals, Prompt-NO decreases.

Fuel-NO is the conversion of inherent nitrogen presents in coal to NO directly and/or through intermediate reaction of HCN and $NH_3$. Figure 11 illustrates the Fuel-NO formation and destruction rate followed by the equation 13a–13d.

Fuel-NO formation rate is shown with positive sign in contour legend, which majorly depends upon the reaction of HCN/NO with $O_2$ to form NO. Figure 13 shows the intensity of HCN and $NH_3$ along the axis at various equivalence ratio cases.

Better conversion of nitrogen to HCN, $NH_3$ and direct NO is obtained in case of higher equivalence ratio as shown in Figure 13. Therefore combustion with a higher equivalence ratio portrays a wider and concentrated NO formation rate as shown in Figure 12. On the other hand, combustion with lower equivalence ratio depicts a narrow but intense Fuel-NO formation rate due to poor HCN, $NH_3$ and NO concentration and intense flame temperature. Dark blue colour in the contour having negative sign depicts the destruction of Fuel-NO that reacts with HCN and $NH_3$ converted to $N_2$.

With the comparison, it is evident that, the Fuel-NO formation rate is higher than other two. Prompt-NO formation rate is much smaller, thus less significant on total NO contribution. From figure 13 it has been observed that, with increase in equivalence ratio, even if there is a better conversion of fuel nitrogen to HCN and $NH_3$ due to rich mixture, but low flame temperature is unable to form much NO. As a result Fuel-NO rate is much higher in case of low equivalence ratio. However a wider range of higher rate of formation of Thermal-NO and Fuel-NO, the concentration of total NO is almost highest in case of φ=3.0 as shown in Figure 9. In the cases of low equivalence ratio (φ=0.8, φ=1.0), even though the formation rate of Thermal, Prompt and Fuel-NO is highest, but limited to a narrow region. Probably higher convection due to very high air velocity causes poor concentration of total NO in the cases of low equivalence ratio (φ=0.8, φ=1.0).

Figure 14a illustrates the NO reburn rate by considering $CH_4$ as reburn fuel. In reburn, NO converts majorly to HCN by reacting with hydrocarbon radical. Thus it is a kind of reverse of Prompt-NO formation. From the Figure, it is observed that, as richness of mixture increases, the rate of

**Table 4.** Maximum and minimum values of temperature and various reaction rates for NO formation and reduction

| | φ = 0.8 | | φ = 1.0 | | φ =3.0 | | φ = 6.0 | | φ = 9.0 | |
|---|---|---|---|---|---|---|---|---|---|---|
| | **Min** | **Max** | **Min** | **Max** | **Min** | **Max** | **Min** | **Max** | **Min** | **Max** |
| Temperature. (K) | 300 | 2178 | 300 | 2204 | 300 | 2091 | 300 | 1957 | 300 | 1930 |
| Thermal-NO rate (kmol/m$^3$-s) | −5.968e-21 | 0.000207 | −9.978e-21 | 0.000214 | −4.4498e-17 | 3.4689e-5 | −1.7643e-10 | 5.4612e-6 | −5.34581e-11 | 3.3557e-6 |
| Prompt-NO rate (kmol/m$^3$-s) | 0 | 4.4034e-5 | 0 | 4. 7924e-5 | 0 | 3.2627e-5 | 0 | 1.9086e-5 | 0 | 1.57849e-5 |
| Fuel-NO rate (kmol/m$^3$-s) | −0.000200 | 0.00225 | −0.000386 | 0.00244 | −0.001010 | 0.00399 | −0.001528 | 0.002133 | −0.000227 | 0.001251 |
| NO Reburn rate (kmol/m$^3$-s) | −3.6817e-5 | 0 | −7.8375e-5 | 0 | −0.001604 | 0 | −0.000275 | 0 | −0.000494 | 0 |

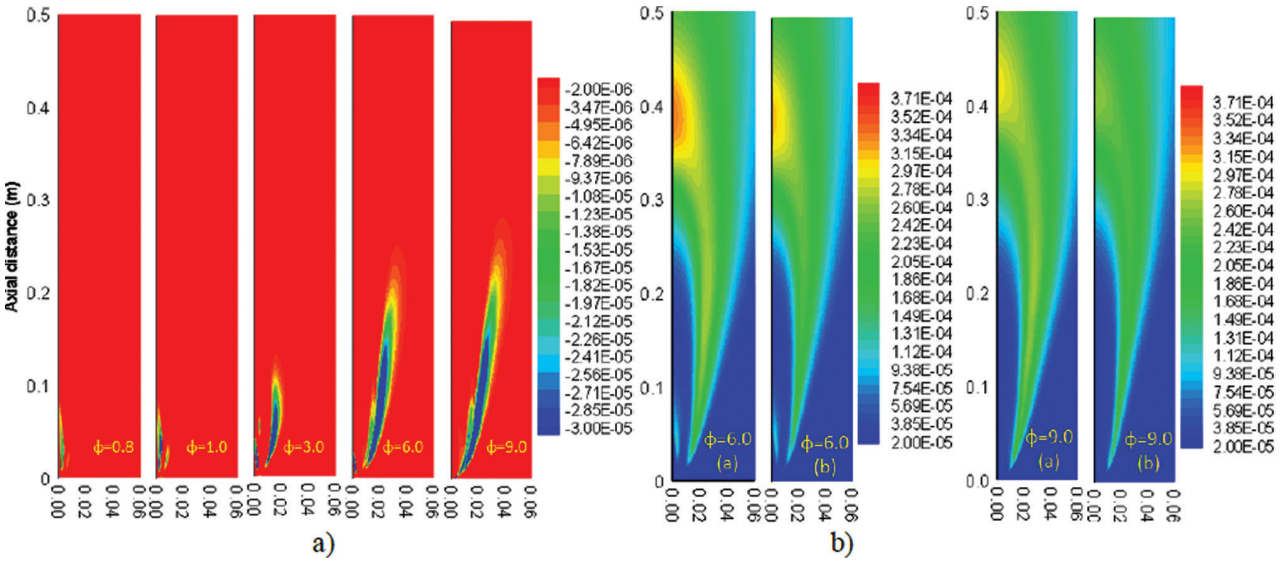


**Figure 14.** a) Reburn reaction rate (kmol/m3-s) for various equivalence ratio condition cases, b) Total NO contour comparison without reburn and with reburn condition for φ=6.0 and φ=9.0.

NO conversion become higher. Because for this condition, the reburn fuel concentration is higher due to slow primary air entrainment. However in this Figure, negative sign represents the destruction of NO. Other factor such as; higher flame temperature also enhances NO reburn rate.

Figure 14b depicts the comparative picture of total NO concentration without considering reburn and with reburn. The comparison for two cases such as; φ=6.0 and φ=9.0 are only given because of significant difference can be visualized easily.

Figure 15a and 15b, depicts the mass weighted average of NO concentration across seven different planes along the axial line with and without reburn respectively for various equivalence ratio conditions. Figure 15a, illustrates the NO reduction efficiency along the axial line. The NO reduction efficiency is calculated as;

$$\text{NO reduction efficiency} = \frac{NO_{\text{without reburn}} - NO_{\text{out reburn}}}{NO_{\text{without reburn}}} \times 100 \quad (21)$$

NO is not reduced significantly with lower equivalence ratio condition due to lower reburn rate. As a result reduction

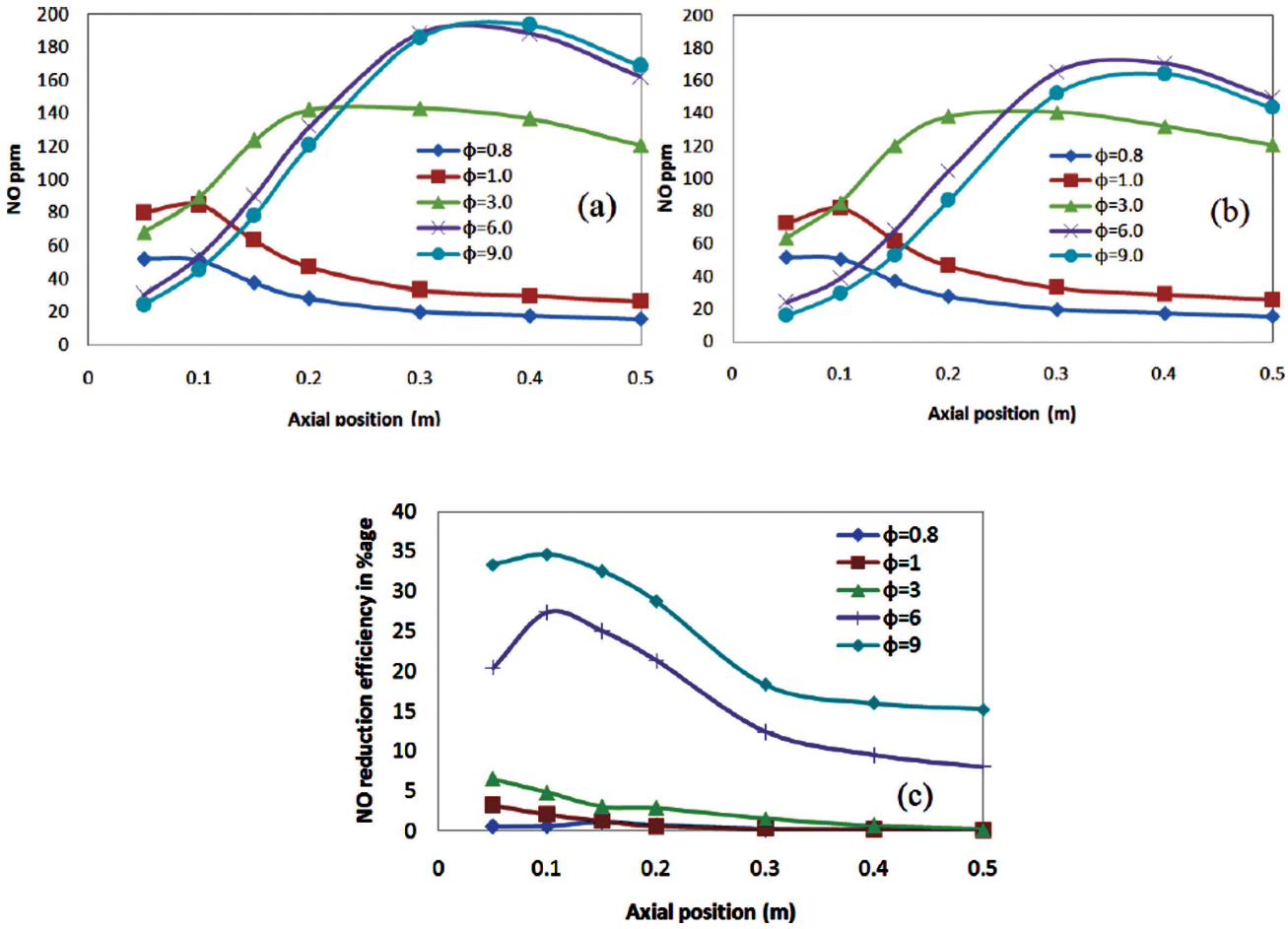


**Figure 15.** a) NO in ppm without reburn, b) NO in ppm with reburn and c) NO reduction efficiency, for various overall equivalence ratio conditions across different axial position.

efficiency decreases throughout along the axis. It is obvious that due to intense reburn rate near inlet region, the reduction efficiency become high at this region. It is decreasing and at outlet plane the reduction efficiency become highest irrespective of equivalence ratio. For φ=9.0, maximum reduction efficiency is around 35% obtained near inlet, whereas at exit plane it is around 15%. But with decrease in overall equivalence ratio, the reduction efficiency suddenly drops. However for φ=0.8, φ=1.0 and φ=3.0 the reduction efficiency is even less than 1% at exit plane. Therefore NO reduction with co-flow reburn method is not much effective for lean mixture condition.

## COAL BURNOUT

Here coal burnout is regarded as, decrease in mass of coal particles due to continuous volatile evolution and char combustion during the movement of particle within the computational domain. Coal burnout percentage across different plane along the axis is calculated as;

$$\text{Coal burnout percentage} = \frac{m_{coal} \times P_{FC} - \left(m_{coal\ outlet} - m_{ash}\right)}{m_{coal} \times P_{FC}} \times 100 \quad (22)$$

Figure 16 illustrates the coal burnout percentage along the length. From the Figure, it is observed that for higher overall equivalence ratio (φ=3.0, 6.0 and 9.0), burnout percentage is around78-85% obtained at exit plane. In these cases, wider temperature field and higher particle residence time due to low air velocity, raise the volatile evolution rate and char combustion as well. On the other hand the as the conditions are reverse for lower equivalence ratio cases, coal burnout percentage decreases in lower equivalence ratio cases. However coal burnout rate increases along the length of the combustor in all the cases. It is obvious that near inlet region, volatile removal and far from inlet the char combustion causes continuous mass losses from coal particle.

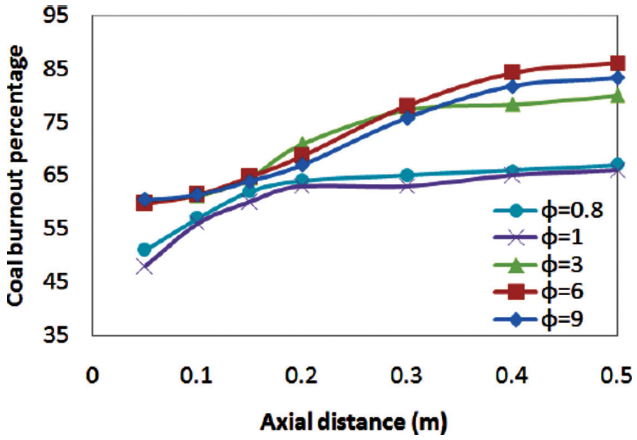


**Figure 16.** Coal burnout percentage for various overall equivalence ratio conditions across different axial position.

## CONCLUSION

A computational simulation has been performed to study the effect of overall equivalence ratio on combustion performance, NO formation and the reburn effect on NO reduction using $CH_4$ as co-flow fuel. A fixed amount of co-flow methane fuel is supplied through an annular space. Through central hole, primary air is supplied along with fixed amount of coal. The required equivalence ratio is maintained by varying the primary air velocity. Thermal-NO, Prompt-NO and Fuel-NO mechanism is used to predict NO formation, whereas equilibrium approach NO reburn model is used for NO depletion. From the study, it is observed that, Fuel-NO contributes a major fraction to the total NO. A significant contribution of Thermal-NO is also there to the total NO. Prompt-NO formation rate is very low; it has negligible contribution to total the NO. From the study it is observed that, for the given geometric conditions, in the case of low equivalence ratio conditions (φ=0.8 and 1.0), even though the rate of formation of Fuel and Thermal-NO is intense but total NO concentration is very low due to narrow reaction zone near inlet. On the other hand due to mixture richness, at higher equivalence ratio cases (φ=3.0, 6.0 and 9.0), the Total NO is much higher and more concentrated away from inlet region.

NO reduction using co-flow methane injection is not an effective method for lower overall equivalence ratio conditions. Because, maximum NO reduction efficiency at φ=0.8, 1.0 and 3.0 is in between 1% to 7%, whereas for φ=6.0 and 9.0, the maximum NO reduction efficiency is around 27% and 34% respectively. Minimum NO reduction efficiency at φ=0.8, 1.0 and 3.0 is around 0.03% to0.8%, whereas for φ=6.0 and 9.0, the minimum NO reduction efficiency is around 15% and 6% respectively. Therefore this NO reduction method is better for highly rich mixture conditions.

## NOMENCLATURE

Symbol

| | |
|---|---|
| $\rho$ | Density |
| $\varphi$ | Enthalpy in energy equation/ species mass fraction for various species in species transport equation |
| $\mu$ | Molecular viscosity |
| $\sigma$ | Prandtl number |
| $\Gamma$ | Diffusivity |
| $Sc$ | Schmidt number |
| $\bar{\tau}$ | Stress tenser |
| $-\bar{\rho}\widetilde{u_i'' u_j''}$ | Reynolds stress tensor |
| $S$ | Source terms |
| $k$ | Generation of turbulent K.E./Kinetic rate |
| $\varepsilon$ | Dissipation of turbulent K.E. |
| $m$ | mass |
| $u$ | Velocity |
| $t$ | time |
| $c_{p_g}$ | Specific heat |
| $h_c$ | Heat transfer coefficient |
| $A_p$ | Projected area of spherical particle |
| $T$ | Temperature |
| $\varepsilon$ | emmisivity |
| $\sigma$ | Stefan Boltzmann constant |
| $\theta$ | Radiation temperature |
| $\Delta H_v$ | Heat formation due to volatile reaction |
| $\Delta H_c$ | Heat formation due to char reaction |
| $f_h$ | Fraction of energy transferred to gas phase formed due to volatile and char reaction |
| $d\Omega$ | Solid angle |
| I | Radiation intensity |
| $R$ | Universal gas constant |
| Y | Species mass fraction |
| MW | Molecular weight |
| $\gamma$ | Stoichiometric air-fuel ratio |
| $p$ | pressure |
| $P_{FC}$ | Mass fraction of fixed carbon obtained from proximate analysis |
| $m_{ash}$ | Mass fraction of ash obtained from proximate analysis |
| $m_{coal}$ | Mass flow rate of coal at inlet |
| $m_{coal\ outlet}$ | Mass flow rate of coal at any cross-section |

Subscript

| | |
|---|---|
| *eff* | effective |
| *lam* | Laminar |
| *tur,t* | Turbulent |
| *g* | gas |
| *s* | solid |
| *m* | mass |
| *p* | particle |
| vol | volatile |
| *i,j* | Directional coordinates/$i^{th}$, $j^{th}$ particle, species. |
| 0 | Initial state |

| | |
|---|---|
| *f* | Fuel, Forward |
| *r* | Reverse |

## AUTHORSHIP CONTRIBUTIONS

Authors equally contributed to this work.

## DATA AVAILABILITY STATEMENT

The authors confirm that the data that supports the findings of this study are available within the article. Raw data that support the finding of this study are available from the corresponding author, upon reasonable request.

## CONFLICT OF INTEREST

The author declared no potential conflicts of interest with respect to the research, authorship, and/or publication of this article.

## ETHICS

There are no ethical issues with the publication of this manuscript.

## REFERENCES


[1] Edge P, Gharebaghi M, Irons R, Porter R, Porter, Pourkashanian M, et al. Combustion modelling opportunities and challenges for oxy-coal carbon capture technology. Chem Eng Res Design 2011;89:1470-1493.

[2] Kuang M, Li Z. Review of gas/particle flow, coal combustion, and NOx emission characteristics within down-fired boilers. Energy 2014;69:144-178. [CrossRef]

[3] Kambara S, Takarada T, Yamamoto Y, Kato K. Relation between functional forms of coal nitrogen and formation of nitrogen oxide (NOx) precursors during rapid pyrolysis. Energy Fuels 1993;7:1013-1020. [CrossRef]

[4] Pershing DW, Wendt J. Pulverized coal combustion: The influence of flame temperature and coal composition on thermal and fuel NOx. Symposium (International) on Combustion 1977;16:389-399. [CrossRef]

[5] Naruse I, Yamamoto Y, Itoh Y, Ohtake K. Fundamental study on N2O formation/decomposition characteristics by means of low-temperature pulverized coal combustion. Symposium (International) on Combustion 1996;26:3213-3221. [CrossRef]

[6] Nichols KM, Thompson LM, Empie Jr HL. A review of NOx formation mechanisms in recovery furnaces. TAPPI J 1991:1-20.

[7] Bell R, Buckingham F. An overview of technologies for reduction of oxides of nitrogen from combustion furnaces. Alexandria: MPR Associates; 2000.

[8] Kurose R, Makino H, Suzuki A. Numerical analysis of pulverized coal combustion characteristics using advanced low-NOx burner. Fuel 2004;83:693-703. [CrossRef]

[9] Zhou W, Moyeda D, Payne R, Berg M. Application of numerical simulation and full scale testing for modeling low NOX burner emissions. Combust Theory Model 2009;13:1053-1070. [CrossRef]

[10] Hu Y, Naito S, Kobayashi N, Hasatani M. CO2, NOx and SO2 emissions from the combustion of coal with high oxygen concentration gases. Fuel 2000;79:1925-1932. [CrossRef]

[11] Li J, Yang W, Blasiak W, Ponzio A. Volumetric combustion of biomass for CO2 and NOx reduction in coal-fired boilers. Fuel 2012;102:624-633. [CrossRef]

[12] Sung Y, Lee S, Kim C, Jun D, Moon C, Choi G,Kim D. Synergistic effect of co-firing woody biomass with coal on NOx reduction and burnout during air-staged combustion. Exp TherFluid Sci 2016;71:114-125. [CrossRef]

[13] Dayton D. Summary of NOx Emissions Reduction from Biomass Cofiring. Technical Report: Summary of NOx Emissions Reduction from Biomass Cofiring. Midwest: National Renewable Energy Laboratory Midwest Research Institute; 2002. [CrossRef]

[14] Su S, Xiang J, Sun L, Zhang Z, Sun X, Zheng C. Numerical simulation of nitric oxide destruction by gaseous fuel reburning in a single-burner furnace. Proceeding of Combustion Institute 2007;31:2795-2803. [CrossRef]

[15] Han X, Wei X, Schnell U, Hein KRG.Detailed modeling of hybrid reburn/SNCR processes for NOx reduction in coal-fired furnaces. Combust Flame 2003;132:374-386. [CrossRef]

[16] Zarnitz R, Pisupati SV. Evaluation of the use of coal volatiles as reburning fuel for NOx reduction. Fuel 2007;86:554-559. [CrossRef]

[17] Wu KT, Lee HT, Juch CI, Wan HP, Shim HS, Adams BR. Study of syngas co-firing and reburning in a coal fired boiler. Fuel 2004;83:1991-2000. [CrossRef]

[18] Choi M, Li X, Kim K, Park Y, Sung Y, Choi G. Analysis of impact factors for exhaust tube vortex flame generation in methane-assisted pulverized coal swirling flames. Appl Therm Eng 2019;157:113550. [CrossRef]

[19] Yamamoto K, Murota T, Okazaki T, Taniguchi M. Large eddy simulation of a pulverized coal jet flame ignited by a preheated gas flow. Proceeding of Combustion Institute 2011;33:1771-1778. [CrossRef]

[20] Franchetti BM, Marincola FC, Navarro-Martinez SN, Kempf AM. Large eddy simulation of a pulverised

coal jet flame. Proceedings of Combustion Institute 2013;34:2419-2426. [CrossRef]
[21] Hwang SM, Kurose R, Akamatsu F, Tsuji H, Makino H, Katsuki M. Observation of detailed structure of turbulent pulverized-coal flame by optical measurement. Fluid Therm Eng 2006;49:1316-1327. [CrossRef]
[22] Hashimoto N, Kurose R, Hwang SM, Tsuji H, Shirai H. Flame. A numerical simulation of pulverized coal combustion employing a tabulated-devolatilization-process model (TDP model). Combust Flame 2012;159:353-366. [CrossRef]
[23] Wen X, Jin H, Stein OT, Fan J, Luo K. Large Eddy Simulation of piloted pulverized coal combustion using the velocity-scalar joint filtered density function model. Fuel 2015;158:494-502. [CrossRef]
[24] Versteeg HK, Malalasekera W. An introduction to computational fluid dynamics: the finite volume method: London: Pearson Education; 2007.
[25] Launder BE, Spalding DB. The numerical computation of turbulent flows. Numerical prediction of flow, heat transfer, turbulence and combustion. Amsterdam: Elsevier; 1983: 96-116. [CrossRef]
[26] Ghose P, Patra J, Datta A, Mukhopadhyay A. Modelling. Prediction of soot and thermal radiation in a model gas turbine combustor burning kerosene fuel spray at different swirl levels. Combust Theory Model 2016;20:457-485. [CrossRef]
[27] Gorenflo R, Mainardi F, Moretti D, Pagnini G, Paradisi P. Discrete random walk models for space–time fractional diffusion. Chem Phys 2002;284:521-541. [CrossRef]
[28] Morsi SAJ, Alexander AJ. An investigation of particle trajectories in two-phase flow systems. J Fluid Mech 1972;55:193-208. [CrossRef]
[29] Ranz WE, MarShal WR. Prog. Evaporation fron DropS-Part I and II.Chem Eng Prog 1952;48:141-146.
[30] Fiveland WA. Transfer H. Three-dimensional radiative heat-transfer solutions by the discrete-ordinates method. Aerospace Research Central US 1988;2:309-316. [CrossRef]
[31] Yu MJ, Baek SW, Kang SJ. Modeling of pulverized coal combustion with non-gray gas radiation effects. Combus Sci Technol 2001;166:151-174. [CrossRef]
[32] Backreedy RI, Fletcher LM, Ma L, Pourkashanian M, Williams A. Modelling pulverised coal combustion using a detailed coal combustion model.Combust Sci Technol 2006;178:763-787. [CrossRef]
[33] ANSYS. ANSYS Fluent Theory Guide. 2011;15317:724-746.
[34] Backreedy RI, Fletcher LM, Jones JM, Ma L, Pourkashanian M, Williams A. Co-firing pulverised coal and biomass: a modeling approach. Proceedings of Combustion Institute 2005;30:2955-2964. [CrossRef]
[35] Magnussen BF, Hjertager BH. On mathematical modeling of turbulent combustion with special emphasis on soot formation and combustion. Symposium International on Combustion 1977;16:719-729. [CrossRef]
[36] Choi CR, Kim CN. Numerical investigation on the flow, combustion and NOx emission characteristics in a 500 MWe tangentially fired pulverized-coal boiler. Fuel 2009;88:1720-1731. [CrossRef]
[37] Fluent A. Academic Research, Release 14.7, Help System, Theory guide. ANSYS; 2014.
[38] De S, SOETE DD G. Overall reaction rates of NO and N2 formation from fuel nitrogen. Pascal Francis 1974;1093-1102. [CrossRef]
[39] Su S, Xiang J, Sun X, Zhang Z, Zheng C, Xu M. Mathematical modeling of nitric oxide destruction by reburning. Energy Fuel 2006;20:1434-1443. [CrossRef]
[40] Leung KM, Lindstedt RP. Detailed kinetic modeling of C1—C3 alkane diffusion flames. Combust Flame 1995;102:129-160. [CrossRef]